scientific reports

Check for updates

OPEN

Low-intensity pulsed ultrasound induces multifaced alterations in chromosome segregation, cytoskeletal filaments and cell junctions

Ion Udroiu[1,10], Federica Todaro[2,3,10], Alessandra Vitaliti[3,10], Damiano Palmieri[4], Eugenia Guida[5], Giulia Perilli[3], Leonardo Duranti[3], Cadia D'Ottavi[3], Maurizio Mattei[6,7], Susanna Dolci[5], Gaio Paradossi[3], Angelico Bedini[8], Ida Silvestri[9], Antonella Sgura[1] & Fabio Domenici[3]✉

Low-intensity pulsed ultrasound (LIPUS) is a widely used non-invasive approach with therapeutic purposes since it provides physical stimulation with minimal thermal effects. The skin epithelium is the first barrier of the human body that interfaces with LIPUS and is subjected to the highest intensity. Little is known about the impact of LIPUS on the skin surface. This work investigates the biological effects of one-hour exposure to 1 MHz LIPUS on human keratinocytes HaCaT and tumoral SK-MEL-28 skin cells. Specifically, we evaluated the cellular state immediately after LIPUS treatment by analyzing cytogenetic endpoints and the response of cytoskeleton and cell junction proteins. Herein we demonstrate that LIPUS induces genomic damage as shown by an increase of chromosome malsegregation and a consequent decrease of cellular proliferation. The mechanical stimulus produced by LIPUS is also transmitted to the cytoskeletal compartment, inducing the expression and re-organization of junction proteins (i.e., E-cadherin and Desmosomes) and intermediate filaments (i.e., F-actin and Cytokeratins) with impact on cell morphology and cell adhesion. These in vitro results highlight the different outcomes following the cytogenetic damage and the resilience response exerted by the cytoskeleton upon mechanical stress, laying the foundation for future in vivo investigations.

Bioeffects induced by ultrasound (US) have been studied for several decades to constantly develop new biomedical applications for therapeutic and diagnostic support[1–6]. It has long been known that high-intensity US can be used to produce thermal effects in biological tissues accompanied by the risk of producing irreversible damage from hyperthermia[7,8]. Alongside this, low-intensity pulsed ultrasound (LIPUS) at medium and high frequency (1–10 MHz) have recently aroused growing interest in biomedical research thanks to their ability to induce mechanical stimuli at cellular and tissue level of potential therapeutic relevance without producing a biologically significant temperature increase[6,9].

LIPUS is generally delivered by an unfocused piezoelectric transducer and transmitted in situ through an aqueous interface (e.g., water, US gel) which allows acoustic coupling between the source and the superficial biological tissue (e.g., skin tissue). In particular, 1 MHz LIPUS produces little or no thermal effects in the

[1]Department of Sciences, Università Roma Tre, Viale G. Marconi 446, Rome 00146, Italy. [2]Section of Endocrinology and Metabolic Diseases, Department of Systems Medicine, University of Rome "Tor Vergata", Rome 00133, Italy. [3]Department of Chemical Science and Technologies, University of Rome "Tor Vergata", Rome 00133, Italy. [4]Medical Physics Unit, Bambino Gesù Children's Hospital, IRCCS, Rome 00165, Italy. [5]Department of Biomedicine and Prevention, University Hospital of Rome "Tor Vergata", Rome 00133, Italy. [6]Interdepartmental Center for Comparative Medicine, Alternative Techniques and Aquaculture (CIMETA), University of Rome "Tor Vergata", Via Montpellier 1, Rome 00133, Italy. [7]Department of Biology, University of Rome "Tor Vergata", Rome 00133, Italy. [8]Department of Technological Innovations and Safety of Plants, Products and Anthropic Settlements (DIT), Italian National Institute for Insurance against Accidents at Work, Inail, Rome 00144, Italy. [9]Department of Molecular Medicine, Sapienza University, Viale Regina Elena 324, Rome 00161, Italy. [10]These authors contributed equally: Ion Udroiu, Federica Todaro, Alessandra Vitaliti. ✉email: fabio.domenici@uniroma2.it

biological medium while maintaining significant and profound transmission of acoustic energy[10]. Overall, the non-thermal effects on the biological target include vibrations and collisions at the aqueous interfaces of cells and tissues[5,10,11]. Depending on the ultrasonic intensity, such effects can involve the presence of cavitating microbubbles at the cellular interfaces, acoustic streaming[5], and, according to Sonophore model[12], at very low pulse intensity (i.e., Spatial Peak Temporal Average, I_{spta}, usually at values lower than 100 mW/cm^2 and Peak Negative Pressure, PNP, in the order of magnitude of 0.1 MPa) LIPUS can result in direct micromechanical stimulation of cell membranes. The non-invasive physical stimulation thus triggered is believed to produce transient alterations in cell[13–15]and tissue permeability, proinflammatory and proliferative responses[16,17], cytogenetic alterations[18,19], and modulation of neuronal transmission[20–24].

A wide range of experiments have been performed on cells and animals leading to useful insights into the biological impact of LIPUS[25–28]. Although this, a clearer picture has yet to be obtained. Preclinical in vivo studies reported in the literature suggest that LIPUS accelerates the healing of fractures and even consolidation in the pseudoarthrosis zone[27]. The effectiveness of LIPUS for soft tissue regeneration and inhibition of inflammatory responses has also been experimentally studied[28]. Furthermore, research has shown that LIPUS is a promising modality for neuromodulation[29]. While many articles have focused on the positive outcomes and effectiveness of LIPUS stimulation, the actual mechanisms underlying LIPUS effects have been much less explored and reported. Among the interpretative difficulties of the reported studies, there is a marked heterogeneity in the protocols and LIPUS setup parameters used. Furthermore, the difference in functions and regulatory mechanisms of the exposed cells made it difficult to draw clear conclusions about the affected pathways[8,30].

Recently, with the increasing attention to LIPUS therapy, more substantial efforts have been made to elucidate the therapeutic mechanisms produced by LIPUS treatments through its in vitro biological effects[31]. Mainly long-term cell alterations involving inflammatory/anti-inflammatory, proliferation, and differentiation have been reported. The major lack of frame of information concerns the cellular state immediately after the LIPUS stimulus, which would better resemble the state of cellular perturbation in connection to long-term effects. In this work, we therefore aim at achieving new data on transient, short-term, alteration of the cell culture, which was detectable as soon as the LIPUS treatment is finished.

It is now known that 1 MHz LIPUS applied at spatial peak temporal average intensity $I_{spta} < 100$ mW/cm^2 is low enough to not cause significant cavitation processes of air bubbles in the aqueous medium while inducing mechanical stress at the cellular level[12,32]. According to Sonophore model[12] during LIPUS treatment the cells can undergo a temporary and significant alteration of the elastic tension of the plasma membrane such as to favor the transient opening of the hydrophilic membrane channels (i.e., transient sonoporation).

Some of us have recently studied the effects on epithelial cell models exposed to LIPUS calibrated at doses (I_{spta} 10-65 mW/cm^2, and exposure times 15–60 min) that are compatible with those programmable in devices for physiotherapeutic and aesthetic use[14,16,32]. In these conditions, progressive transient differential effects with dose including morphological-positional changes and alteration of membrane permeability were revealed, the latter considered an experimental confirmation of Sonophore model[32]and paving the way to perspectives in drug delivery[33,34]. Alongside this, and of particular note by setting of a LIPUS exposure time limit of 1 h and I_{spta} of 65 mW/cm^2, slight alterations in proliferation were reported with a decrease in phosphorylated Signal Transducer and activator of Transcription 3 (STAT3) and an increase in BCL-2-associated X protein (BAX)/B-cell lymphoma 2 (BCL-2) gene expression with the triggering of apoptosis[16]. On the other hand, under the same treatment conditions, also a significant transient increase in the level of IL-6 via NfKb was revealed, suggesting that the majority of treated cells can resume proliferation[16]. More importantly, in recent studies on human fibroblasts and human tumor cells (HeLa and MCF-7) undergoing low-intensity 1 MHz US (~70 mW/cm^2) an increase in mitotic abnormalities (including multipolar spindles) was found[35,36]. The combination of these endpoints suggests that the elastic tension produced by US on the plasma membrane[12,15]may also involve the anchoring junction proteins capable of transducing the mechanical signal to the filaments of the cytoskeleton and the mitotic spindle[37,38].

It has indeed emerged that mechanical stimuli and more generally the level of elastic tension of the extracellular matrix (ECM) can produce resilience responses which result in the modulation of the expression of junction proteins[39–43]. This could mean that if US can produce a non-thermal, temporary, and locoregional modification of the mechanical characteristics of the cellular environment, mitotic cells can sense it and transduce the mechanical tension even on the tubulin of the spindle poles. The latter perturbation may trigger a cascade of cytogenetic and proliferative changes, including the risk of development and differentiation of tumor cells. In this way, US-induced micromechanical stress could induce differential and, apparently, contrasting effects depending on the state of the cell cycle and the type of cells involved. This appealing hypothesis has led us to study on epithelial cell models the conditions of significant appearance of pivotal endpoints documented in the literature (e.g., aneuploidy phenomena, cell cycle proliferation response) in conjunction with possible alterations of the cytoskeleton and the mitotic spindle. Of particular importance is the understanding of the bioeffects on the skin epithelium which is subjected to the highest intensity during LIPUS treatments, and where an activation of resilience responses to the mechanical stimulus is expected together with proinflammatory, and proliferative alterations[38]. Skin cancer cells might also be stimulated by mechanical inputs such as those induced by LIPUS. Particularly in malignant melanoma which is the most aggressive type of skin cancer, it has been recently reported that the micromechanical environment, also in interconnection with keratinocytes, influences the growth and physiological dynamics of the tumor tissue[44].

Bearing these aspects in mind, the ultimate and ambitious goal would be to transform LIPUS into a powerful biomedical technology capable of influencing the cellular and intercellular state in a safe and non-invasive way. To date, this progress suffers from the lack of literature aimed at understanding the LIPUS interaction with the cytoskeletal and cell junction network. To fill the gap, as a first step of comprehension, we focused on human keratinocytes HaCaT, and tumorigenic SK-MEL-28, both undergoing 1-hour exposure to 1 MHz LIPUS (I_{spta}

below 100 mW/cm^2) to study immediate cytogenetic endpoints and the related response of junction proteins and intermediate filaments. Moreover, we have considered the concomitant presence of possible short-term proliferation effects. In particular, we have pointed out the mitotic cycle together with the level of pivotal mitotic regulator cyclin CCNB1, whose level of expression, nuclear translocation, and activation of nuclear cyclin B1-CDK1 complex is related to the activation of spindle checkpoints, also affecting the malignant phenotype and proliferation of tumors; we also monitored the executor of cell death protease, Caspase 3, and of proliferation and reorganization of cytokeratins, IL-6.

On both HaCaT and SK-MEL-28 skin cell lines, we show herein robust evidence of significant US-triggered alterations of the mitotic spindle, with concomitant effects involving the expression and organization of junction proteins and intermediate filaments. All this evidence not only confirms that 1 MHz acoustic fields of biomedical relevance at low, subcavitation regimes, can interfere with the stability of the mitotic spindle, but they produce a mechanical stress that is sensed and transmitted through the adherens junctions (AJ) and the cytoskeleton to which the spindle is hooked. These may turn into a transient impact on proliferation, cell cycle, and IL-6-mediated proinflammatory response.

Materials and methods

Cell lines and culture conditions

The immortalized human keratinocyte cell line, HaCaT, and the human melanoma cell line SK-MEL – 28 were obtained from Interlab Cell Line Collection (ICLC, National Cancer Research Institute, Genoa, Italy). Cells were grown in Dulbecco's Modified Eagle's Medium (DMEM, Corning, NY, USA) supplemented with 10% heat-inactivated fetal bovine serum (FBS), 2 mM L-glutamine (Corning, NY, USA), non-essential amino acids (Gibco, Thermo Fisher Scientific, Waltham, MA, USA), 100 U/ml penicillin and 100 µg/ml streptomycin (Corning, NY, USA) and incubated at 37 °C, in a humidified atmosphere with 5% CO_2.

LIPUS exposure

The in vitro exposure setup has already been described in detail in previous works[14]. Briefly, the US exposure equipment consists of a waveform generator (Agilent 33220 A, Agilent Technologies, Santa Clara, CA, USA), a signal amplifier (Amplifier Research 25A250, Telford, PA, USA) and a non-focused, submersible, piezo-ceramic US transducer tuned at 1 MHz (Precision Acoustics Ltd, Dorchester, UK). The system can produce well-defined sinusoidal US waves independently from the exposure conditions and allow for generating signals with different intensities, both in continuous and pulsed modes. The transducer is placed at the bottom of a tank ($30\times30\times30$ cm^3) filled with degassed Milli-Q water (18.2 MΩ cm, resistivity). To isolate the effects of progressive waves from the reflected ones, the tank was coated with acoustic absorbers (Aptflex F28, Precision Acoustics Ltd, Dorchester, UK). The temperature of the water bath was kept constant at 25 °C. The temperature inside and outside the Petri dish was monitored using a digital thermometer (Checktemp4, Hanna instruments, Woonsocket, RI, USA.), i.e., for the LIPUS exposures involved herein temperature oscillations within 1 °C were revealed. All parameters characterizing the performance of the transducer were measured by a needle hydrophone of 0.5 mm diameter (Precision Acoustics, Dorchester, UK) with sensitivity 483 mV/MPa at 1 MHz endowed with a micrometric positioning system and coupled to a booster amplifier (coupler DC with integrated power supply, Precision Acoustics Ltd, Dorchester, UK) and an oscilloscope (Philips, Amsterdam, NL). The calibration curves of the US field were determined inside Petri dishes with micrometric step-size movements to determine the point of maximum peak-to-peak pressure next to the Petri bottom surface (where the cells were grown), previously filled with 3 mL of cell culture medium. The overall exposure configuration geometries were set to avoid matching the resonance length of the US stimulus. Moreover, the US setup was checked concerning the presence of pulse repetition frequencies and the sinusoidal waveform compared to that of the US source to exclude the generation of multiple harmonics.

By calibration, we can measure the US pressure and, ultimately, the intensity of the US that the cells onto the Petri undergo. In this work, the US intensities were calculated in terms of Spatial Peak Temporal Average, I_{spta}, (i.e., the maximum spatial intensity measured when the pulse is activated, averaged for the period of pulse repetition). This quantity is commonly used in the characterization of the biological effects induced by low-intensity US.

For LIPUS treatments the cells were first seeded on 35 mm diameter, ~0.90 mm bottom thicknesses, polystyrene Petri dishes (Falcon® Easy Grip, Becton Dickinson Labware, Franklin Lakes, NJ; © ibidi GmbH, Martinsried, Germany) with a density of $3–4\times10^4$ cells/dish. After 24 h, the dishes were closed with parafilm and then immersed in water, just under the surface, in line with the transducer at an SSD of 7 cm (where near-field US effects can be negligible). LIPUS Irradiations were applied in a pulsed regime (period 300 µs, duty cycle 10%) at a frequency of 1 MHz at varying intensities below 100 mW/cm^2 that is for general consensus the cavitation threshold (i.e., I_{spta} =18 ± 2 mW/cm^2, 30 ± 3 mW/cm^2, 65 ± 5 mW/cm^2, 85 ± 8 mW/cm^2, 160 ± 10 mW/cm^2) and at a fixed exposure time of 1 h. Calibration curves and details are reported in Section S1 of Electronic Supplementary Material (ESM).

Cytokinesis-block micronucleus test with anti-kinetochore antibodies

One day before irradiation, 50,000 cells were seeded inside 35 mm Petri dishes. Cytochalasin-B (final concentration: 3 µg/mL in DMSO, Sigma-Aldrich, Merck Life Science, Burlington, MA, USA) was added immediately after irradiation. Twenty-four hours after irradiation, cells were fixed with cold methanol and air dried. Slides were then washed in PBS and kept in a blocking solution (Bovine Serum Albumin, BSA 1%) for 30 min. Subsequently, cells were incubated with CREST antikinetochore antibody (Antibodies Incorporated, Davis, CA, USA) diluted 1:1 in BSA 1% for 1 h at 37 °C. Slides were then washed with BSA 1% and PBS before adding FITC-conjugated anti-human antibody (Sigma Aldrich, St. Louis, MO, USA) diluted 1:80 in BSA 1%. After a final wash in PBS,

cells were stained with 1 μg/mL of DAPI (4′,6-diamidino-2-phenylindole, Sigma Aldrich, St. Louis, MO, USA). Cells were scored at 63× magnification using a Zeiss Axiophot (Carl Zeiss, Oberkochen, Germany) microscope with ultraviolet light (359 nm excitation filter; 441 nm barrier filter) and classified for kinetochore staining (using 494 nm excitation filter, 523 nm barrier filter) as either CREST-positive or CREST-negative micronuclei. Micronuclei (MN) frequencies were assessed scoring 500 binucleated cells (BNC) for each sample. Percentage of BNC (BNC/total cells) was also assessed as a measure of proliferation.

Analysis of mitotic index

One day before irradiation, 50,000 cells were seeded inside 35 mm Petri dishes. Immediately after sonication, cells were fixed in ice-cold methanol for 5 min, air-dried and then stained with DAPI (Sigma Aldrich, St. Louis, MO, USA). Cells were scored at 63× magnification, as above. Mitotic index was calculated counting the number of mitoses in 300 cells in each sample. The ana-telophase / pro-metaphase ratio (A + T / P + M) was assessed counting 100 mitoses in each sample.

Analyses of mitotic spindles

One day before irradiation, 50,000 cells were seeded inside 35 mm Petri dishes. Immediately after sonication, cells were fixed in ice-cold methanol for 5 min and then air-dried. Subsequently, cells were blocked using BSA 5% for one hour at room temperature. Afterwards, cells were incubated overnight at 4 °C in a wet chamber with 1:400 mouse antibody for α-tubulin (Sigma Aldrich, St. Louis, MO, USA) and 1:1000 rabbit antibody for γ-tubulin (Sigma Aldrich, St. Louis, MO, USA) in 5% BSA. Successively, cells were incubated for 1 h at 37 °C in 1:200 anti-mouse Alexa Fluor 546-conjugated antibody (Life technologies, Carlsbad, CA, USA) and 1:200 anti-rabbit Alexa Fluor 488-conjugated antibody (Scientific, Life technologies, Carlsbad, CA, USA) for α- and γ-tubulin, respectively. Finally, cells were counterstained with DAPI (Sigma Aldrich, St. Louis, MO, USA). Cells were scored at 63× magnification, as above. Percentages of spindle anomalies were assessed counting one hundred mitoses per sample.

Fluorescence microscopy

Confocal laser scanning microscopy was performed using the inverted confocal microscope Nikon Eclipse (Ti-E C1) equipped with an Argon ion laser (Spectra Physics, Mountain View, California) (emission wavelength 488 nm) and He-Ne laser (Melles Griot, Florence, Italy) (emission wavelength 543 nm). Images were acquired with a 100x oil immersion objective (N.A.: 1.3, 0.07 μm/px ratio, 0.13×0.13 mm^2) using EZ-C1 software, version 3.91.

Wide-field fluorescence microscopy was performed with a Nikon Eclipse Ti inverted microscope supplied with an Andor Zyla 4.2 sCMOS camera (Andor Instruments, Belfast, Northern Ireland) using a mercury vapor lamp as light source and B2A filters (wavelength pass excitation filter band: 450–490 nm; "cut-on" wavelength of the high-pass dichroic mirror: 500 nm, "cut-on" wavelengths of the high-pass barrier filter: 515 nm) and G2A (d bandpass excitation filter wave: 510–560 nm; high-pass dichroic mirror cut-on wavelength: 565 nm, high-pass barrier filter wavelengths: 590 nm cut-on), using a 60x (N.A.: 1.4, 0.11 μm/px ratio, 0.22×0.22 mm^2) and a 100x oil immersion objectives.

Immunofluorescence analysis

Cells were grown on coverslips and exposed to US as previously described (see Ultrasound exposure setup and experimental protocol paragraph).

After irradiation, cells were washed three times in PBS and fixed with 4% paraformaldehyde (Corning, NY, USA) for 15 min at room temperature. Cells were then washed twice in PBS, permeabilized for 10 min with a solution of PBS/Triton X-100 0.1% (v/v) and incubated for 1 h with PBS/BSA 5% (v/v). Cells were then incubated overnight at 4 °C, in a humidified chamber with the following antibodies: anti-Cytokeratin (Dako, Agilent Technologies, Santa Clara, CA, USA, AG-M351529-2, 1:200), anti-Desmosome (Novus Biologicals, Bio-Techne, Minneapolis, MN, USA, NBP2-81279, 1:100), anti-Caspase3 (Antibodies, Abcam, Cambridge, UK, A25544, 1:100), anti-CyclinB1(Invitrogen, Thermo Fisher Scientific, Waltham, MA, USA, PA5-120418, 1:100), anti-beta Actin (Novus Biologicals, Bio-Techne, Minneapolis, MN, USA, NB-600-505, 1:200) and Alexa fluor 488 Phalloidin conjugated Antibody (Invitrogen, Thermo Fisher Scientific, Waltham, MA, A12379). After washing, secondary antibody (Alexa Fluor 594 goat anti mouse IgG, Alexa Fitch 488 goat anti rabbit IgG, Jackson ImmunoResearch, West Grove, PA, USA, 1:200) was added for 1 h at room temperature and washed twice in PBS. Afterwards, coverslips were mounted with Fluoro-Gel II (Electron Microscopy Sciences, Hatfield, PA, USA) containing DAPI for nuclei staining. Deconvolution and microscopy inspections were performed as described in the fluorescence microscopy paragraph. Images were acquired and processed with NIS-Elements software (Nikon-Europe B.V. Rome, Italy). The fluorescence intensity was analyzed using Image J software (NIH Image, Bethesda, MD, USA): the densitometry of 10 randomly selected fixed squares from the cytoplasm and nucleus of single cells was measured and the values were obtained in arbitrary units showing the average optical density of each square, from which the average values were calculated.

Fe-SEM

Field Emission Scanning Electron Microscope (FE-SEM) images were performed on a Zeiss Leo SUPRA™ 35, Carl Zeiss SMT (Oberkochen, GE) in collaboration with the "Materials and Devices for Energy at University of Rome Tor Vergata" group.

The instrument allows a resolution of: 2.1 nm at 1 kV, 1.3 nm at 15 kV and 1.0 nm at 20 kV; with a high voltage range between 100 V and 30 kV. The Gun is a Schottky Field Emission Gun with an emission current between

4pA and 20nA and a magnification factor between 20X and 900,000X. It is also endowed of a backscattering detector.

Sputter: before observing the samples at FE-SEM they were subjected to metallization in an RF Emitech K550x sputter using gold targets (Au target), sputtering was performed for 1:30 min at 25 mA to obtain a coating homogeneous thick about 10 nm. HaCaT cells grown on borosilicate coverslip within Petri dishes and the 1 MHz US treatments were performed for 1 h at $I_{spta} = 65 \pm 5$ mW/cm^2 (that we call LIPUS exposure) and at significantly higher $I_{spta} = 160 \pm 10$ mW/cm^2 (that we call positive-treated samples). Thereafter both the treated samples and non-treated samples (negative non-treated controls) were fixed using 3.6% (v/v) formalin in PBS maintained at 4 °C and then incubated with the cells for 30 min at room temperature. All samples were fixed on stubs using carbon tape and then sputtered.

Profilometry of the Fe-SEM images was processed by Gwyddion software (Ver. 2.62).

Preparation of samples and Western blot analysis

After US exposure, cells were harvested, washed in PBS and incubated for 20 min on ice in lysis buffer containing 50mM HEPES (H3375 Sigma Aldrich, St. Louis, MO, USA), 1% Triton X-100 (T8787 Sigma Aldrich, St. Louis, MO, USA), 10 mM $MgCl_2$ (M8266 Sigma Aldrich, St. Louis, MO, USA), 10% glycerol (G5516 Sigma Aldrich, St. Louis, MO, USA), 100 mM NaCl (S7653 Sigma Aldrich, St. Louis, MO, USA), 0.5 mM dithiothreitol (DTT) (D9779 Sigma Aldrich, St. Louis, MO, USA), 10mM β -glycerophosphate (G9422 Sigma Aldrich, St. Louis, MO, USA), 0.5 M sodium orthovanadate (450243 Sigma Aldrich, St. Louis, MO, USA) and protease inhibitors cocktail (PPC1010 Sigma Aldrich, St. Louis, MO, USA). The samples were then centrifuged at 1000 × g for 20 min at 4 °C and the supernatant was collected. The protein concentration was determined using the BCA Protein Assay kit (Thermo Fisher Scientific, Waltham, MA, USA). The samples were diluted in Laemmli Buffer 2X, plus 5% β-mercaptoethanol and denatured at 95° C for 5 min. Proteins (20–50 µg) were separated by SDS-PAGE in 4–20% gradient gels (BIO-RAD, Hercules, CA, USA) or in uniform gels of 10% polyacrylamide and transferred to PVDF membrane (Amersham, Buckinghamshire, UK). The membrane was blocked in a solution of TBS-Tween 20 (TBST) with the addition of BSA 5% (v/v) or 5% milk 5% (v/v) for 1 h at room temperature. Incubation with primary antibodies was carried out at 4 °C overnight in TBST- BSA 5% (v/v) and then with the appropriate horseradish peroxidase-conjugated secondary antibody (Santa Cruz, Biotechnology, Santa Cruz, CA, USA). The horseradish peroxidase conjugate was detected by chemiluminescence with an ECL kit (Clarity western ECL substrate BIO-RAD, Hercules, CA, USA) and auto-fluorography. Primary antibodies used for immunodetection, as well as their dilutions, are listed in Table 1. Full-length blots are reported in Section S4 of ESM.

Statistical analysis

Results were reported as mean value ± standard deviation (SD) of measurements obtained by at least three independent experiments ($n = 3$). Statistical significance was evaluated by Student's t test, using the GraphPad Prism software (GraphPad Software, San Diego, CA, USA) and a p-value < 0.05 was considered significant ($^*p < 0.05$; $^{**}p < 0.01$; $^{***}p < 0.001$).

Results

HaCaT and SK-MEL-28, representative models of human skin keratinocyte and melanoma cells respectively, were treated for one hour by 1 MHz LIPUS. We first quantified the cytogenetic effects at varying the ultrasound intensity (18–85 mW/cm^2, I_{spta}). Then, fixing the exposure condition at the highest LIPUS stress where the aneugenicity of LIPUS was confirmed in HaCaT cells, we investigated the response of both cell lines on junction and intermediate filaments able to sense and transmit the mechanical stress wave to the cytoskeletal network and mitotic spindle. Finally, some short-term effects on proliferation are evidenced.

Effects on genome integrity

In order to assess the possible genomic damage exerted by LIPUS, we performed the Cytokinesis-Block Micronucleus test with CREST staining (i.e., with anti-kinetochore antibodies). With this method, micronuclei can be classified as resulting from either acentric fragments (and thus, not containing a kinetochore, MN-, Fig. 1A) or whole chromosome loss (and thus, containing a kinetochore, MN+, Fig. 1B). Sonication of HaCaT cells resulted in significant increases of MN + frequencies (Fig. 1C). Also in SK-MEL-28 cells, sonication induced

Antibody	Name Specification	Dilution
Actin	A2066 (Sigma)	1:2000
β -Actin	NB-600-505 (Novus Biologicals)	1:2000
β -Catenin	sc-59,737 (Santacruz)	1:1000
E-Cadherin	ab11512 (Abcam)	1:1000
Caspase3	A25544 (Antibodies)	1:500
Cyclin B1	PA5-120418 (Invitrogen)	1:500–1:100
Cytokeratin	AG-M351529-2 (Dako)	1:500
Desmosome	NBP2-81279 (Novus Biologicals)	1:500

Table 1. Primary antibodies used for Western blot analysis.

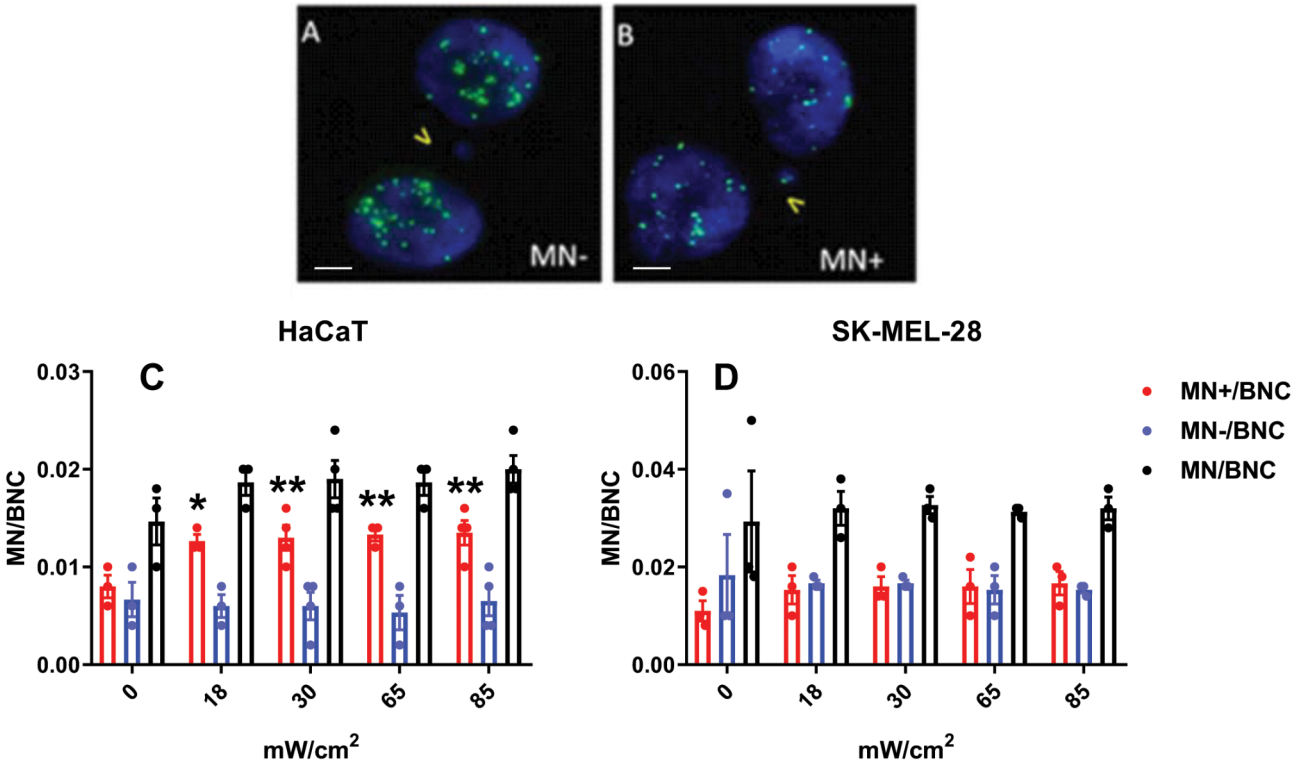

Fig. 1. Micronucleus test with CREST staining. Representative images of a binucleated cell with CREST-negative micronucleus (MN-, **A**) and binucleated cell with CREST-positive micronucleus (MN+, **B**); kinetochores are stained in green, DNA in blue; Scale bar: 5 µm. Frequencies of CREST-positive (MN+), CREST-negative (MN-) and total micronuclei (MN) per binucleated cell (BNC) in HaCaT (**C**) and SK-MEL-28 (**D**) cells. Bars represent mean ± SD. Points represent values of each sample. Asterisks represent significant differences with unsonicated samples (*$p < 0.05$; **$p < 0.01$).

an increase of MN + frequencies, but the differences with the unsonicated samples were not significant (Fig. 1D). For both cell lines, frequencies of MN- in the sonicated cells were almost identical to the ones of the unsonicated samples.

With the aim of confirming the aneugenic nature of the damage occurred in sonicated HaCaT cells, we investigated the frequency of spindle aberrations in cells exposed to the highest dose (i.e., 85 mW/cm^2). Sonicated cells showed a significant increase, about twice, in spindle abnormalities compared to untreated cells (Fig. 2).

Effects on actin filaments distribution, cell attachment and morphology

To study cytoskeletal filaments, we performed CLSM and fluorescence microscopy measurements using Phalloidin conjugated antibody to mark F-Actin. We found that HaCaT and SK-MEL- 28 cells exposed to US (1 MHz, I_{spta} = (85 ± 8) mW/cm^2) showed a different organization of the F-actin filaments (Fig. 3A and B, and Figure S3A and B of ESM) that was not correlated to a change in the content of F-actin after the LIPUS treatment. Indeed, the fluorescence intensity of Phalloidin was comparable in control and treated cells (Figure S3C and D of ESM). Upon US exposure, a change in the spatial distribution of the F-actin occurred in both cell lines, with diffusion and thickening of actin fibers both in the central perinuclear area and in the lateral perimembrane. The cellular morphology appeared changed (ESM, Figure S3). In particular, the plasma membranes of treated HaCaT cells were significantly more rounded compared to the control (Figure S3A).

To further investigate morphological alterations, we decided to use a scanning electron microscope to obtain ultrastructural analysis on HaCaT cells where the changes in the distribution of Actin filaments together with cell shape deformation seemed comparatively higher. To have more robust information on the variations detected by FE-SEM, we performed LIPUS treatments not only at comparable LIPUS dose but also at a significantly higher intensity (I_{spta} = 160 mW/cm^2) for 1 h, considering the latter treatment as a "positive control" concerning the LIPUS-induced mechanical stress that we would observe in HaCaT cells. The ultrastructural analysis (Fig. 3 and Section S3.1 of ESM) confirmed the CLSM observation, highlighting the progressive retraction and flattening of the cell protrusions and microvilli of the surface of treated cells (Fig. 3C central and right panels) as the applied US intensity increased, with the strongest effect at 160 mW/cm^2 (Fig. 3C right panel).

Furthermore, in the treated cells, we found fewer compact areas with the presence of breaks in the cell-cell junctions (Fig. 3D central and right panels). These alterations became progressively more evident as the intensity of the US increased. These effects were not revealed in the control sample (Fig. 3D left panel).

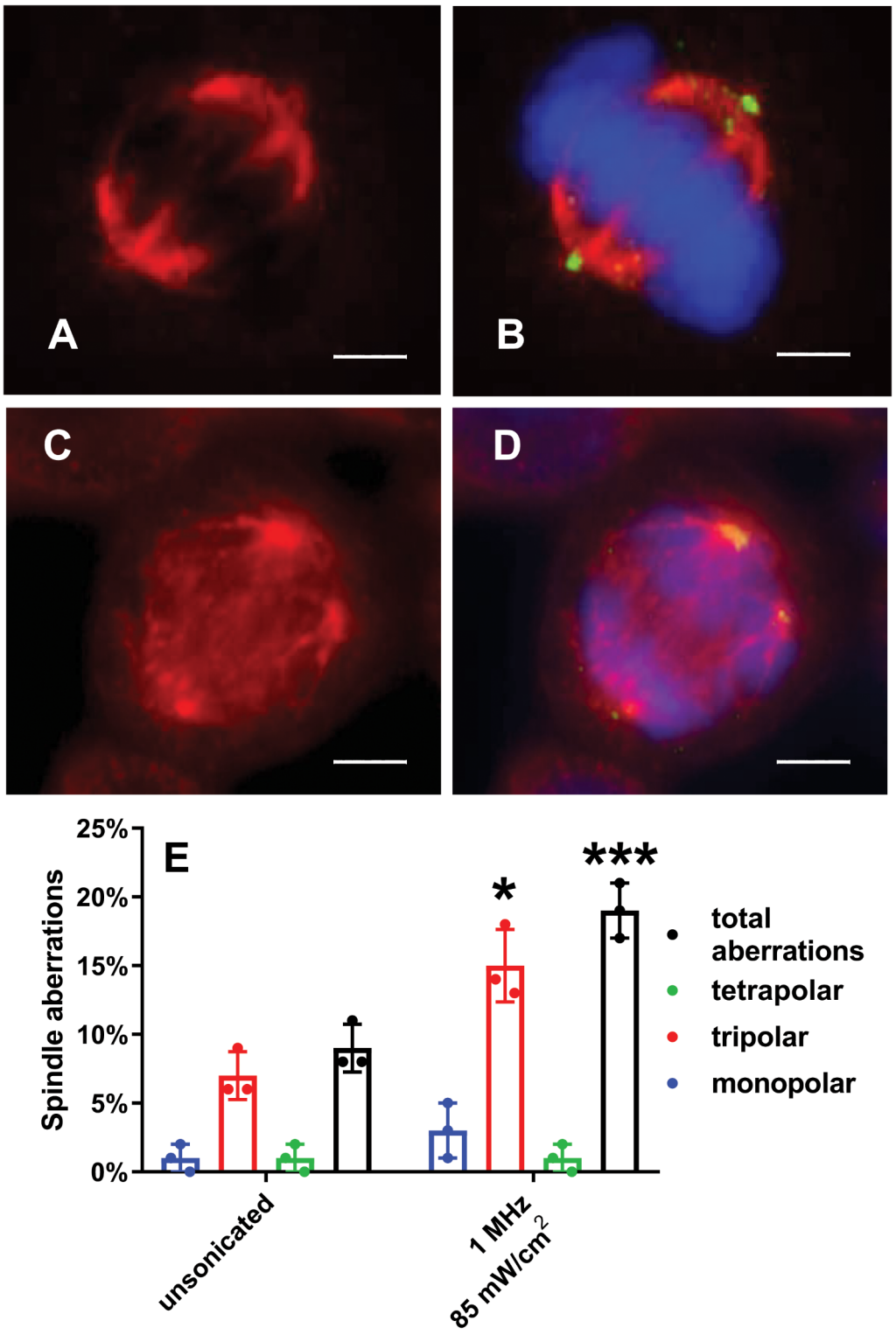

Fig. 2. Abnormalities of the mitotic spindle. Representative images of a normal metaphase (**A**-**B**) and a tripolar anaphase (**C**-**D**): **A**, **C** anti-α-tubulin antibodies (in red) showing the shape of the mitotic spindle; **B**, **D** same image showing also spindle poles (in yellow) and chromosomes (in blue). Scale bar: 5 µm. **C** Frequencies of spindle aberrations in unsonicated and 85 mW/cm^2-sonicated HaCaT cells. Bars represent mean ± SD. Points represent values of each sample. Asterisk represents significant difference with unsonicated samples (*$p < 0.05$; ***$p < 0.001$).

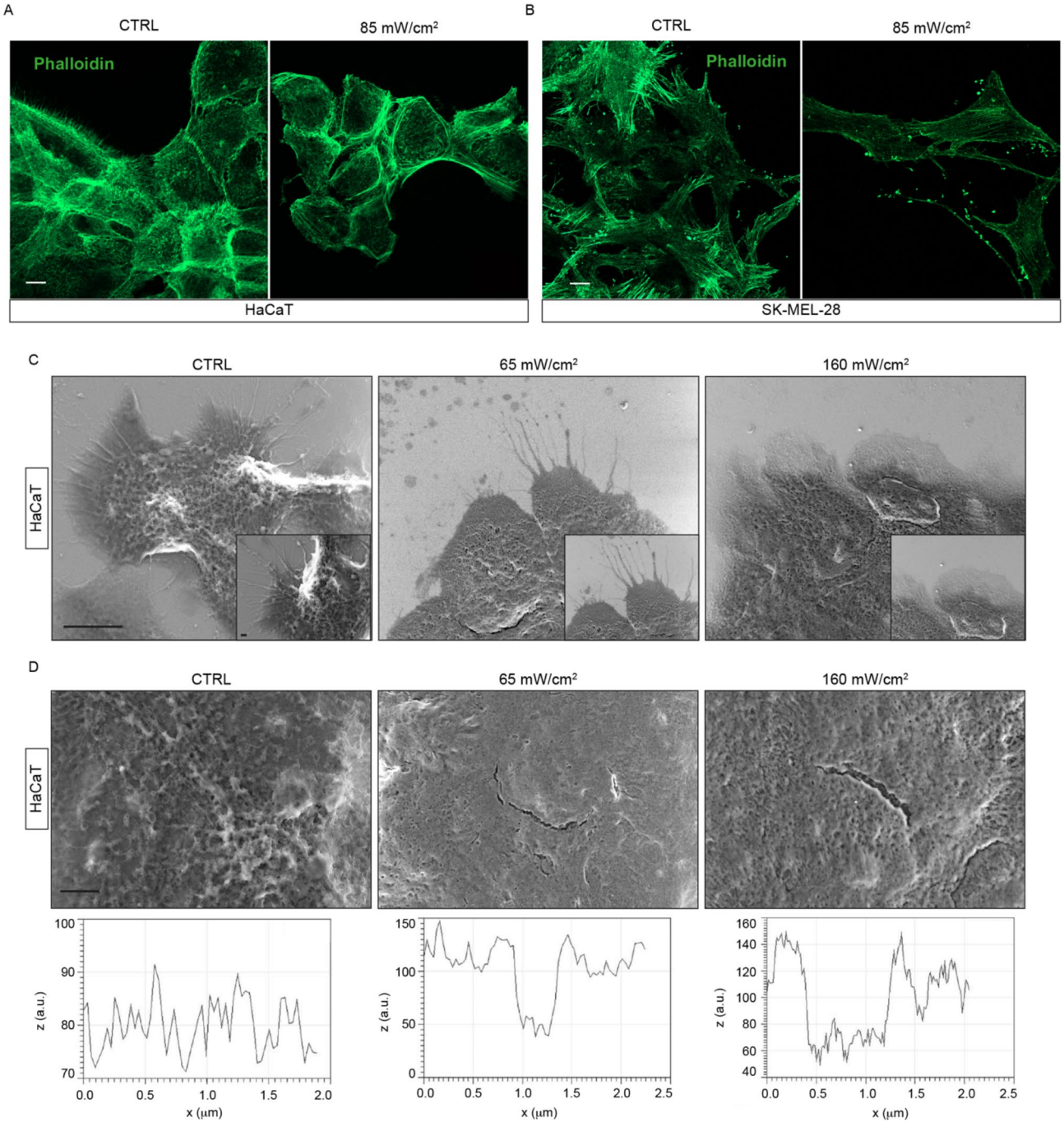

Fig. 3. Effects of LIPUS exposure on F-actin filaments and cell adhesion. Confocal fluorescence of Phalloidin immunolocalization (green) in HaCaT (**A**) and SK-MEL-28 cells (**B**) treated for 1 h with 85 mW/cm^2 US (right) compared to control (left); scale bar 10 μm. **C** FE-SEM images of HaCaT cells: non-treated cells (left), exposed to LIPUS (65 mW/cm^2, middle), and positive-treated control (160 mW/cm^2, right). Scale bars: main images: 10 μm, bottom right images 1 μm. **D** FE-SEM images of HaCaT cell fractures following US irradiation: control (left), 65 mW/cm^2 (middle), 160 mW/cm^2 (right). Scale bar: 10 μm. Bottom graphs: profilometric analysis highlighting the breaks in the treated cells (65 mW/cm^2, middle; 160 mW/cm^2, right).

In the bottom panels of Fig. 3, the profilometric analysis highlighted the presence of breaks in cells after both LIPUS exposure and comparatively higher I_{spta} (positive control). Using the Gwyddion software, the average length and width of the cracks were obtained, considering an average of 15 different line profiles per membrane "wound". For the LIPUS exposed samples, an average length of 7.2 ± 0.3 m and an average width of 0.3 ± 0.1 m were obtained, while for the positive-treated control, an average length of 9.7 ± 0.3 m and an average width of 0.5 ± 0.1 m were obtained. This demonstrates that the plasma membrane fractures correlated with the US intensity. A more complete profilometric analysis including roughness and porosity of the plasma membrane of

HaCaT is reported in ESM (Sect. 3.2, Table S1) also highlighting a slight increase in average roughness after the LIPUS exposure.

These results, together with the morphological studies suggest that US can interfere with the structure of the plasma membrane and therefore could also perturb the mechanical signaling that the cytoskeletal filaments physiologically activate for cell-cell adhesion.

Effects on adherens junctions and desmosomes

To better understand the effects of LIPUS on cell-cell contacts we focused our attention on different cellular junctions. Specifically, we started by investigating the impact on AJ. Indeed, the ternary E-cadherin/β-catenin/αE-catenin complex, which constitutes AJ, can modulate cellular stiffness proportionally to the force applied to cells activating a mechanosensitive signal transduction pathway[45]. The extracellular region of E-cadherin extends from the cell surface to bind adjacent cells whereas its intracellular region interacts with catenins. Specifically, β-catenin links cadherin to F-actin through α-catenin, thus transmitting mechanical forces directly to cytoskeleton, turning in AJ protein aggregation and stabilization of cell-cell adhesion in epithelial barrier[46].

Upon 1 h LIPUS exposure at I_{spta} = 85 mW/cm^2, western blot analyses showed that β-catenin level increased significantly in HaCaT cells while its amounts remained unaffected in SK-MEL-28 (Fig. 4A and B). Furthermore, LIPUS did not induce a significant modulation of e-cadherin levels both in HaCaT and SK-MEL-28 cells (Fig. 4A and C).

Next, we investigated the impact of LIPUS on the stability of desmosomes in the reference cell models. The modulation of the expression of proteins of the desmosome complex can affect intercellular adhesion junctions and the effectiveness of the intracellular mechanical tension sensory module (TSM)[40]. Alteration of desmosome

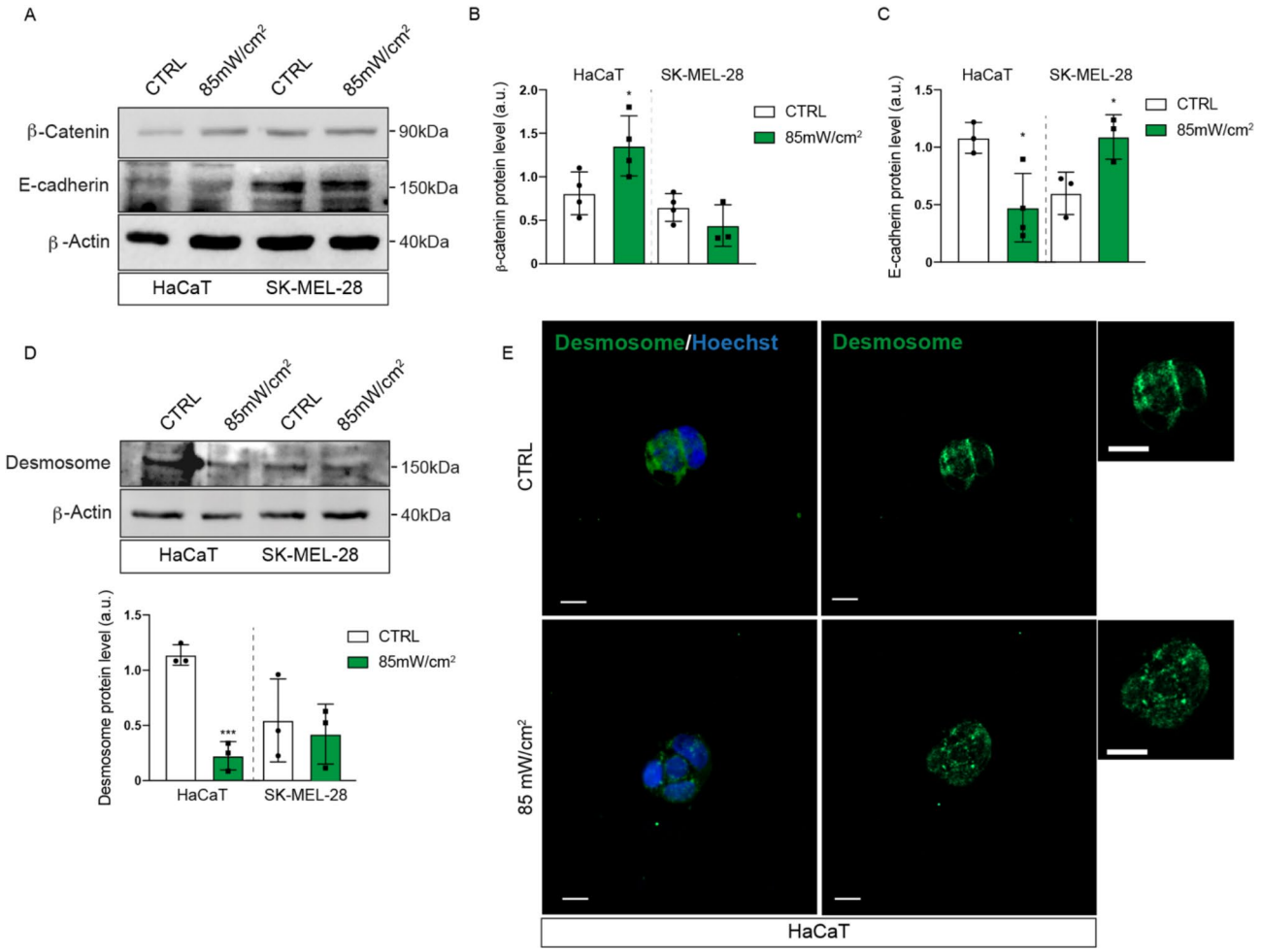

Fig. 4. Adherens junctions and desmosomes are modulated by LIPUS. **A** β-catenin and E-cadherin protein levels obtained by western blot analysis of cells following 85mW/cm^2 LIPUS irradiation. **B** and **C** Densitometric analysis of β-catenin and E-cadherin levels. **D** Western blot of Desmosome levels in LIPUS exposed HaCaT and SK-MEL-28 cells. β-Actin was used for protein levels normalization. One representative blot is shown for each antigen, data are presented as a mean ± SD ($n \geq 3$, Student's t-test $^*p < 0.05$; $^{***}p < 0.001$). **E** Immunofluorescence analysis of Desmosome in HaCaT cells. Magnification 100X; scale bar 10 µm. Full-length blots are shown in ESM (Section S4, Figure S6).

proteins can therefore influence the expression and organization of intermediate filaments and even the organization of cortical actin filaments[39,40].

Interestingly, upon irradiation, protein levels of desmosomes decreased in HaCaT cells, whereas in SK-MEL-28 cells, we did not observe significant change with respect to unexposed cells (Fig. 4D). Moreover, in HaCaT cells, we investigated the cellular distribution of desmosomes after US exposure by using CLSM. After treatment, desmosomes appeared as delocalized proteins within cytoplasm, instead in unexposed cells they were mainly localized at cell edges (Fig. 4E).

Effects on cytokeratin expression and distribution

It has been reported that cytokeratins network can be reorganized by cells to alter their mechanical properties and to sustain their integrity[47]. Therefore, we examined cytokeratins contribution to the mechanical resilience in collaboration with desmosomes. Interestingly, after irradiation of HaCaT cells, cytokeratin levels increased (Fig. 5A and C) with a change in their cellular distribution. Indeed, as shown in Fig. 5B, cytokeratins were localized closer to the nucleus as compared to unexposed cells.

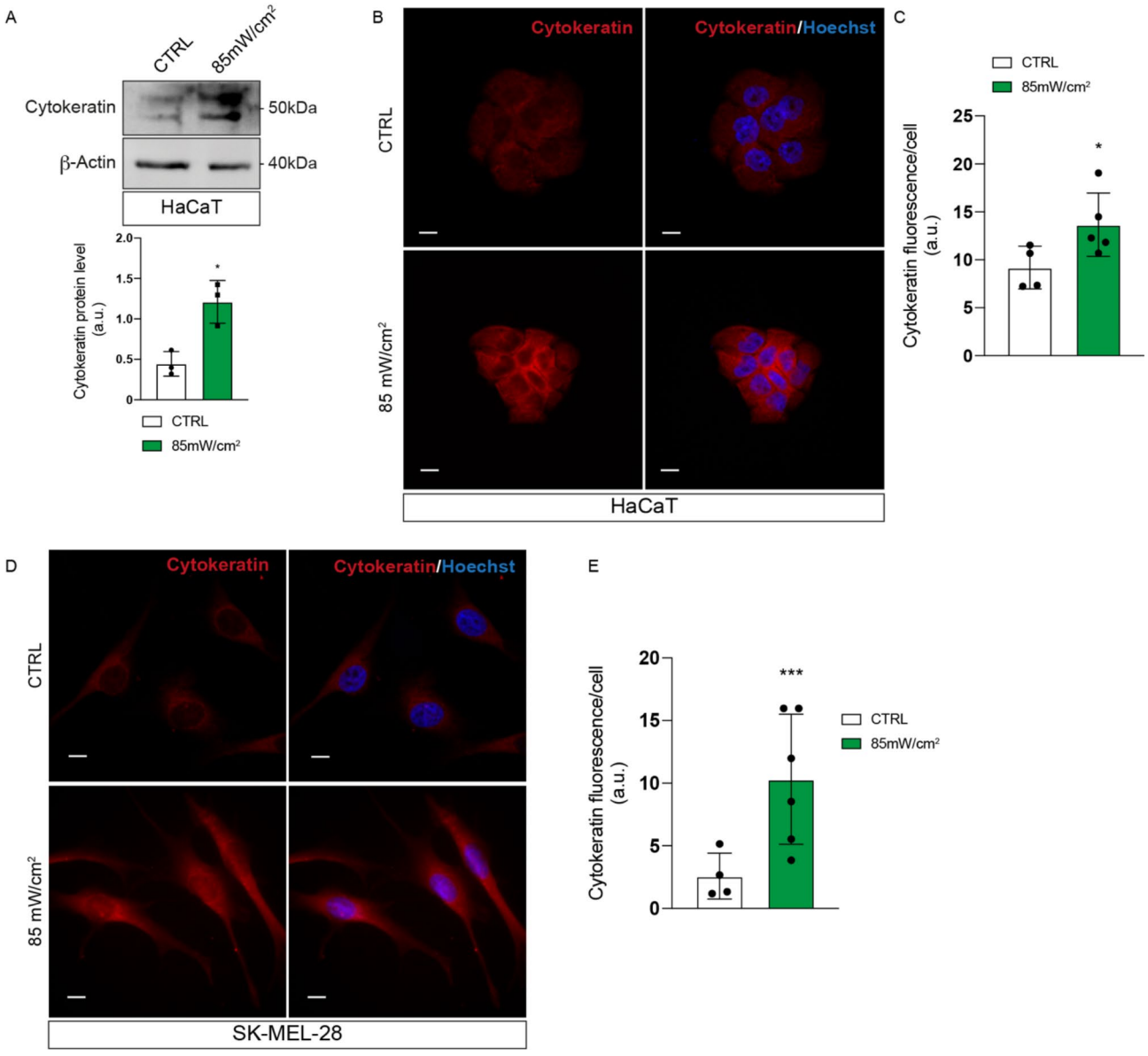

Fig. 5. Analysis of cytokeratin levels and distribution upon LIPUS exposure (**A**) Western blot (upper) and densitometric analysis (lower) of cytokeratin in HaCaT cells. β-Actin was used as loading control. Immunostaining for cytokeratin in HaCat (**B**) and SK-MEL-28 (**D**) cells and the corresponding densitometric analysis (**C** and **E**). Both cell lines are shown after treatment with 85 mW/cm^2 LIPUS. One representative blot/image is reported for each antigen, data are presented as a mean ± SD ($n \geq 3$, Student's t-test $^*p < 0.05$; $^{***}p < 0.001$). Magnification 100X; scale bar 10 µm. Full-length blot is shown in ESM (Section S4, Figure S7).

Regarding SK-MEL-28 cells, we found that US exposure only increased cytokeratin expression without affecting their cellular distribution (Fig. 5D and E).

Effects on cell proliferation

In the same samples in which we scored MN frequencies, we also assessed the percentages of BNC out of total cells as an index of cellular proliferation. Sonication caused a dose-dependent decrease of the percentages of BNC (Fig. 6). Compared to unsonicated samples, the decrease was statistically significant in HaCaT cells exposed to 85 mW/cm^2 and in SK-MEL-28 cells exposed to 65 and 85 mW/cm^2.

In order to verify if the changes in proliferation were associated with perturbations of the mitotic progression, we assessed the mitotic index. While in HaCaT cells a significant increase on the samples sonicated with 85 mW/cm^2 was shown (Fig. 7A), in SK-MEL-28 cells no difference is revealed (Fig. 7B). We also brought to light a dose-dependent decrease of the ana-telophase / pro-metaphase ratio (A + T / P + M). In particular, compared to unsonicated samples, the decrease was statistically significant in HaCaT cells exposed to 65 and 85 mW/cm^2 (Fig. 7C) and in SK-MEL-28 cells exposed to 85 mW/cm^2 (Fig. 7D).

Analysis of cyclin B1 and Caspase-3

Mitotic delay can result in different cellular fates such as cell division, cell death or mitotic slippage[48]. One of the most important regulators of cell division is the Cyclin-dependent kinase 1 (CDK1)-CyclinB1 complex. Thus, we decided to monitor the levels of Cyclin B1 upon US irradiation to define which route was taken by our cell models. Interestingly, after 1 h exposure to 1 MHz LIPUS at I_{spta} = 85 mW/cm^2 a decrease of cyclin B1 levels was shown in both cell systems, even if the reduction was significant only in HaCaT cells as demonstrated by western blot and immunofluorescence analysis (Fig. 8A, B and C).

Moreover, we analyzed the modulation of Caspase-3 which is the Cyclin B1 partner to control cell fate (i.e., the choice between cell death and mitotic slippage is mediated by the balance between these two proteins). Specifically, upon irradiation, an increase in Caspase-3 levels concomitant to the decrease of Cyclin B1 in both cell lines was detected (Fig. 8D, E and F).

Discussion

General significance of the study

The bioeffects of Low-Intensity Pulsed Ultrasound on human cells are a topic of growing interest in biomedical research. Based on recent in vivo literature, LIPUS seems to affect various cellular processes including proliferation, differentiation, and healing[17,28]. However, despite advances in understanding the involved mechanisms, in vitro studies investigating the effects of LIPUS on human cells are still lacking. The absence of adequate in vitro studies limits our understanding of the detailed biophysical mechanisms through which LIPUS interacts with human cells. Thus, further in vitro research is needed to clarify the impact of LIPUS on different human cell lines and to identify potential biomolecular targets involved in its biophysical effects. These studies could provide a solid foundation for the development of targeted LIPUS therapies for a variety of pathological conditions, from osteoporosis to tissue regeneration. More importantly, they can provide information on cellular responses capable of producing unwanted alterations during the healing process.

In this study, we examined the effects of 1 MHz LIPUS treatment on HaCaT and SK-MEL-28 cell lines, as non-tumorigenic and tumorigenic models of human skin. In particular, HaCaT is the well-consolidated in vitro model of the keratinocyte barrier, the latter being formed by the main cells in direct contact with the LIPUS transducer. Thus, it is crucial to understand whether and how these waves can affect the genomic stability of

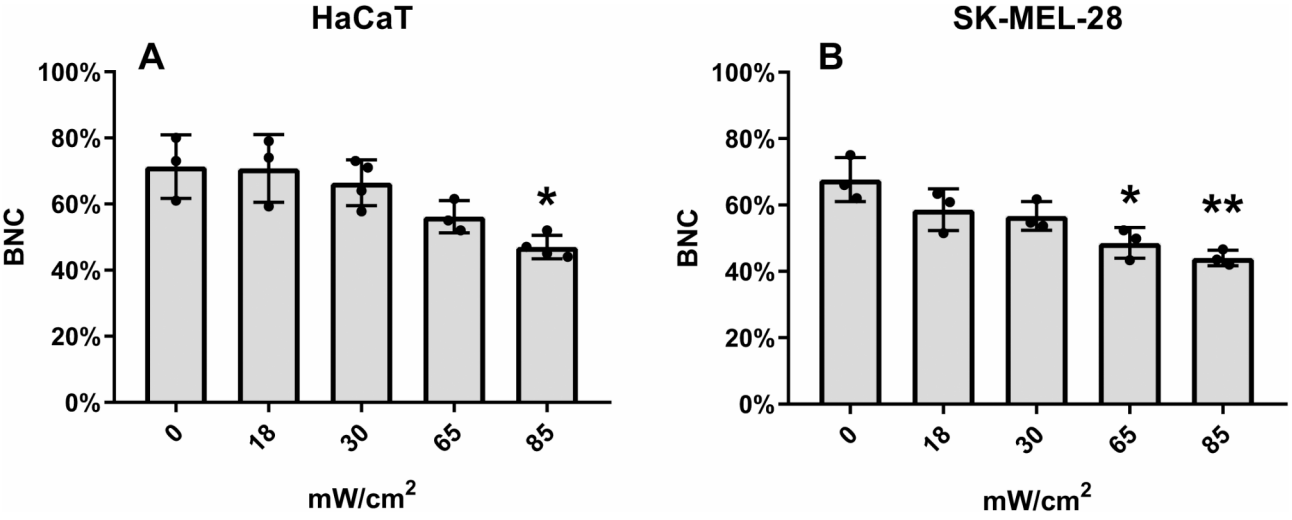

Fig. 6. Percentages of binucleated cells. **A** HaCaT cells; **B** SK-MEL-28 cells. Bars represent mean ± SD. Points represent values of each sample. Asterisks represent significant differences with unsonicated samples (*$p < 0.05$; **$p < 0.01$).

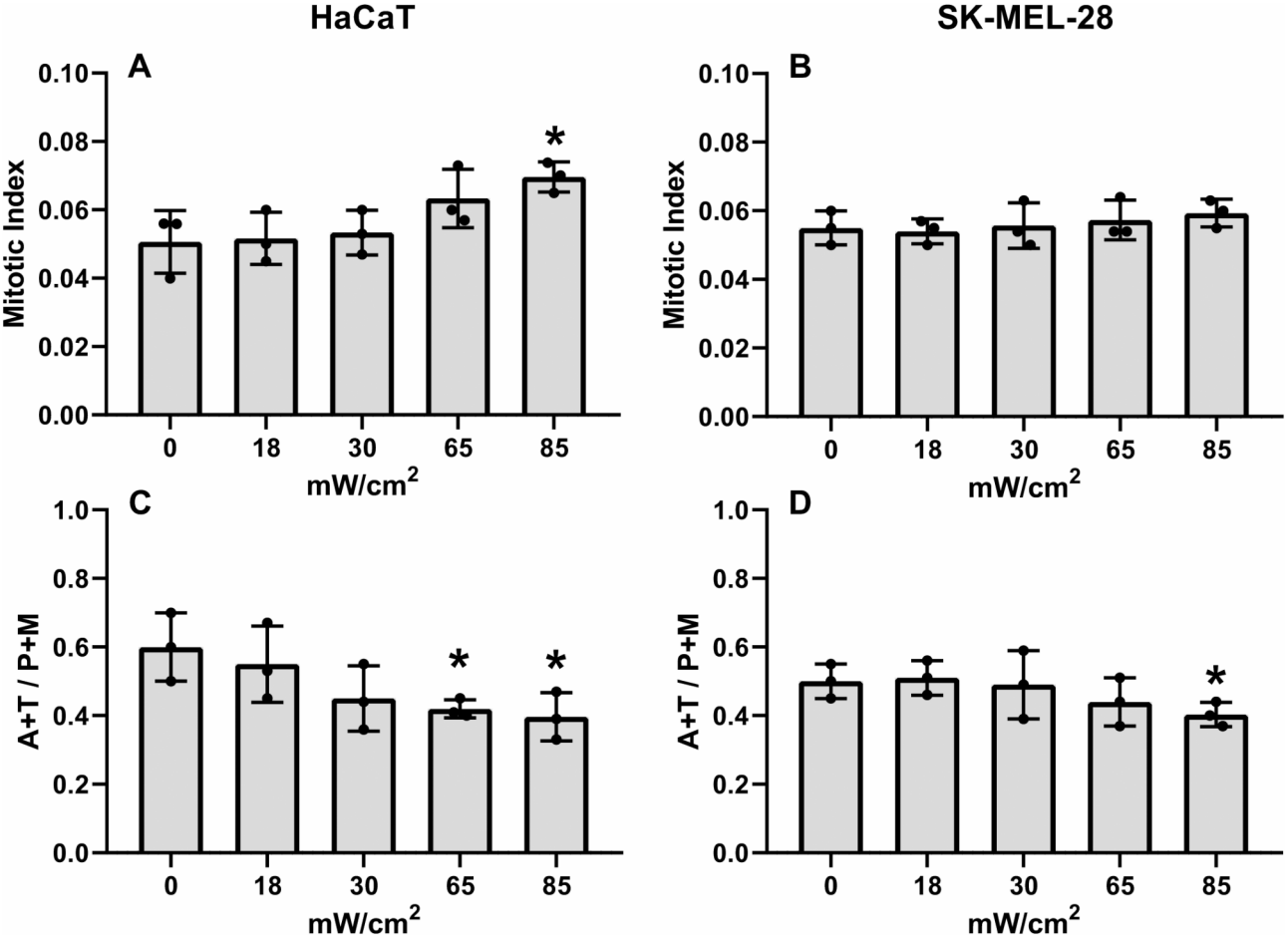

Fig. 7. Mitotic indices. Mitotic index in HaCaT (**A**) and SK-MEL-28 cells (**B**). Ana-telophase / pro-metaphase ratio (A + T / P + M) in HaCaT (**C**) and SK-MEL-28 cells (**D**). Bars represent mean ± SD. Points represent values of each sample. Asterisks represent significant differences with unsonicated samples (*$p < 0.05$).

epithelial cells as well as stimulate changes at the level of junction proteins and intermediate filaments and the consequences on proliferation. Previous studies have suggested that LIPUS treatment may induce mechanical stress on cells, but the impact at the cytogenetic level related to the cytoskeleton protein remains to be determined. Our investigation seeks to address this gap in knowledge by exploring whether LIPUS treatment may trigger chromosomal abnormalities, and, under the conditions of relevant exposures, highlighting concomitant significant alterations of the intermediate filaments. According to previous literature[16], we set the exposure time to 1 h, which would favor the accumulation of alteration events, thus facilitating the unveiling of cytogenetic alterations and corresponding cytoskeletal alterations. We discuss herein that the mechanical stimulus not only produces stress at the level of the mitotic spindle but is transmitted and alters the network of filaments connected to it, i.e., causing stress at the level of the junctions, and therefore cell morphology with impact on cell viability and cell cycle progression.

LIPUS impairs chromosomal segregation

We confirmed past studies[35,49] observing that US below the cavitation threshold does not induce clastogenic damage (CREST-negative micronuclei in our case, Fig. 1). This is due to the fact that DNA breakage is exerted by US through the formation of reactive oxygen species[49]and these are produced only through cavitation[50].

On the other hand, one-hour exposure to 1 MHz LIPUS produced an increase in the frequencies of CREST-positive (i.e., derived from aneugenic damage) micronuclei (Fig. 1). The aneugenic nature of the damage induced by LIPUS was also demonstrated by a significant increase of spindle anomalies in exposed cells compared to untreated ones (Fig. 2). Thus, this is the result of the action of LIPUS on the mitotic spindle, which is made up of microtubules. As tubulin can be (to different degrees) disassembled by US[51,52], sonication determines abnormalities of the mitotic spindle[36], leading to chromosome malsegregation and the formation of MN[35].

Ultrasonic mechanical forces are sensed through the network of actin filaments

It is reasonable to hypothesize that the alteration of the cytoskeleton could derive from the propagation effect of the elastic field through the cytoskeletal filaments. It is known that the cytoskeletal cross-talk between actin filaments and microtubules drives the assembly of cellular structures, the formation and propagation of the

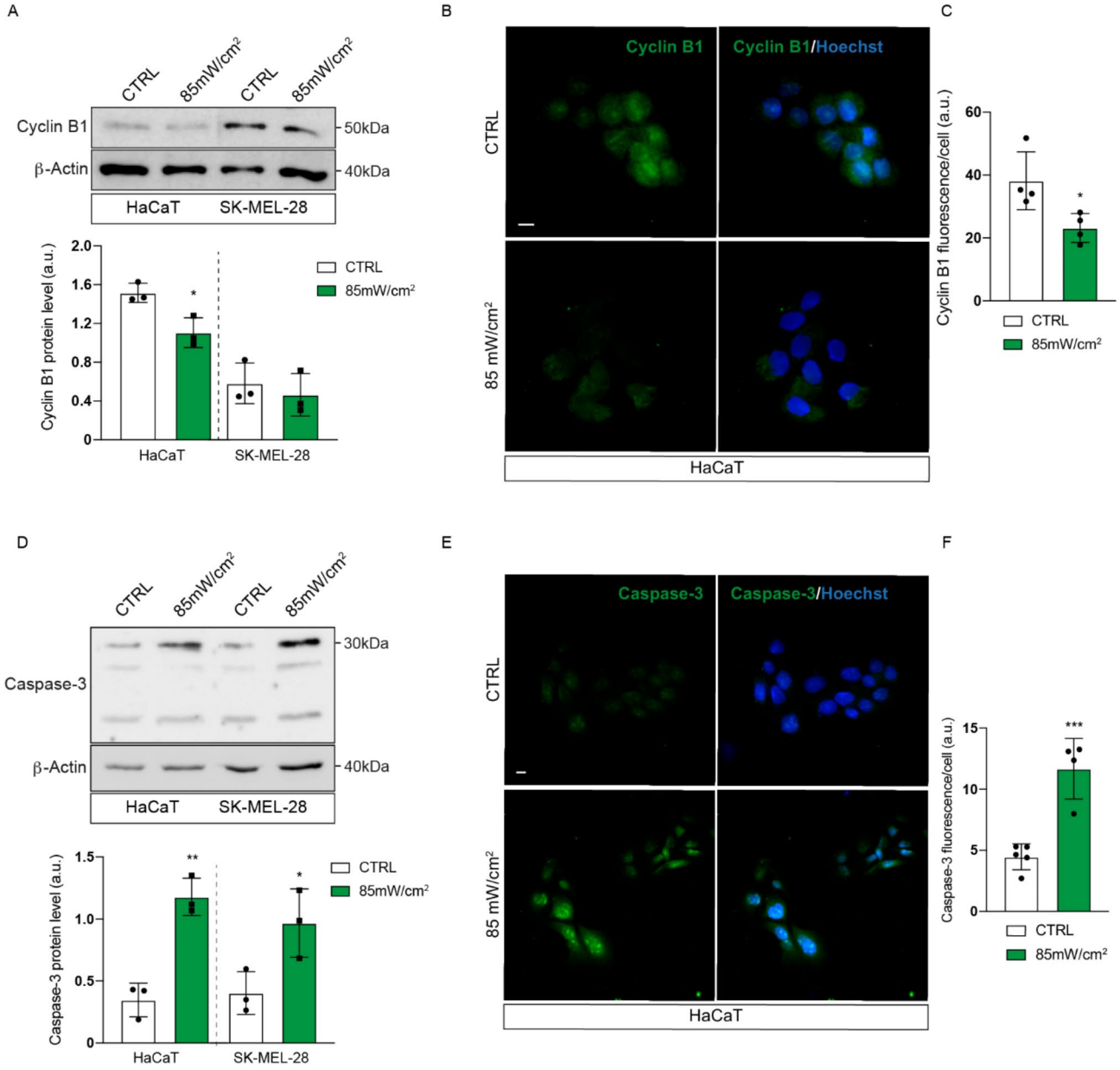

Fig. 8. Effects of LIPUS treatment on Cyclin B1 and Caspase-3 levels. **A** The levels of Cyclin B1 were measured by western blot in HaCaT and SK-MEL-28 cells (upper) and quantified by densitometric analysis (lower). **B** Immunodetection of Cyclin B1 in HaCaT cells and **C** its corresponding signal analysis (magnification 100X; scale bar 10 μm) **D** Western blot analysis of Caspase-3 in HaCaT and SK-MEL-28 cells. The related densitometric analysis is reported below. **E** Immunofluorescence analysis of Caspase-3 and **F** its quantification in HaCaT cells (magnification 60X; scale bar 10 μm). All experiments were performed at the following setup: 85 mW/cm^2 for 1 h. One representative blot/image is reported for each antigen, data are presented as a mean ± SD ($n \geq 3$, Student's t-test $^*p < 0.05$; $^{***}p < 0.001$). Full-length blots are shown in ESM (Section S4, Figure S8).

mitotic spindle and chromosome congression and segregation. The actin filaments behave as mechanically tunable cell backbone and the mechanical stress can modify their conformation, the binding and the regulatory action of the actin-binding proteins[53]. As reported in literature[54–56], profound changes in actin filaments induced by mechanical and vibrational impact, turn out into cytoskeletal rearrangement thus coercing variations in cell morphology and volume. The changes in cell shape found here are confirmed by the change in the spatial distribution of the Actin-F filaments as evidenced by immunofluorescence (Fig. 3, and Figure S3 of ESM). The impact in the organization of the filamentous actin suggests that the mechanical stress produced by the LIPUS stimulus induces a cellular "resilience" response which manifests itself through a cellular shape alteration depending on the type of cells involved as highlighted by the FESEM and CLSM images (Fig. 3). Of particular note, the treated HaCaT cells, unlike the SK-MEL-28, appear to assume a more rounded shape (Figure S3A of

ESM). Variations in cell shape towards a more rounded one under similar LIPUS exposure conditions have previously been reported on HaCaT keratinocytes[16,55] in which a recovery of HaCaT to the native form was concomitant with the triggering of a proinflammatory process via NfKb. As reported in the introduction, in this work our efforts were thus channeled into adding new information on the state of alteration at the moment immediately after the LIPUS stimulus. Both epithelial cell lines showed that LIPUS mechanical stress produces an alteration of the mitotic spindle, resulting in malsegregation, together with an alteration of the spatial organization of the actin filaments. Given that, not all cells showing the F-actin alteration are in the meta/anaphase stage. Therefore it is reasonable to hypothesize that the oscillatory pressure stimulus that propagates from the extracellular aqueous matrix inside the cell can produce morphological cytoskeletal variations that modify the mechanical tension of the mitotic spindle during the chromosome segregation phase.

On the other hand, the idea that targeting the actin filaments can impair cellular transformation and biological processes such as cell division and cell migration is not new[57–59]. It is known that in this way it is possible to inhibit the proliferation of tumor cells including epithelial melanoma cells. Despite this, it is very difficult pharmacologically to discern between the actin cytoskeleton of tumor cells and the actin filaments the latter being involved in tumor cell survival. In this regard, the significant disorder induced by LIPUS on actin filaments of SK-MEL-28 being connected to cytogenetic alteration will deserve dedicated attention.

LIPUS can stimulate minimal cadherin-catenin complex in adherens junctions

It is well known in the literature that the LIPUS stimulus can create structural and membrane permeability alterations which can be transient or lethal to the cell depending on the dose and mechanical index of the ultrasonic stimulus. The impact of this alteration on the interconnected cytoskeleton is less clear until now. It has recently emerged that mechanical stress on ECM induces profound remodeling of junction proteins connecting with cortical filaments of actin and keratin[39]. In particular, AJ and desmosomes can convey mechanical stress at the intracellular level, modulate the repositioning of cells, and stimulate processes of migration, proliferation, and differentiation[39]. A direct route of transduction of plasma membrane tension to the cytoskeleton is through modulation of the binding strength of the minimal cadherin-catenin complex with F-actin. Such cooperative binding regulates dynamic cytoskeletal connections in epithelial tissues[41,42].

Our results (Fig. 4) in both epithelial cell lines indicate that an oscillatory mechanical LIPUS stimulus is able to alter significantly the expression of the E-Cadherin cell-cell adhesion protein, which play a key role in transducing mechanical information to F-actin. Down-regulation and upregulation of E-Cadherin have been often associated with stimulation or inhibition, respectively, of the cell cycle and proliferation in the epithelial barrier[60]. Indeed, our work demonstrated that HaCaT keratinocytes, analyzed immediately after LIPUS treatment, showed a decrease in E-cadherins paralleled by an overexpression of β-catenin, both significant (Fig. 4). β-catenin is a multitasking molecule with adhesive-structural and signaling activities. Force measurements reported in the literature demonstrate that the interaction with actin is strengthened under mechanical load[60,61]. In this frame, newly synthesized β-catenin is immobilized by E-cadherin in AJ, where it can also interact with α-catenin, thus indirectly modulating actin filaments. In greater detail, mechanical tension promotes the strong binding state of actin with the α-catenin- β-catenin complex, by favoring the recruitment of vinculin, and, in turn, a catch bond behavior[60].

On the other hand, just after LIPUS stress, β-catenin may be released from AJ to act as a transcriptional factor in the canonic Wnt signaling pathway (which by blocking the activity of degradation, produces, in fact, increased levels of cytoplasmic β-catenin)[62]. According to the opposite expression of E-cadherins and β-catenin, LIPUS treatment induced on HaCaT cells a significant interplay between Wnt signaling and cell-cell adhesions, that can result in the destabilization of AJ promoting cell migration and differentiation[63]. Noteworthy, the activation of the Wnt pathway in cancer cells is associated with antiapoptotic response and oncogenic activity[61].

In cancer cells, loss of E-cadherin is often related to an increase in cell metastatic behavior. However, in the last decade, novel roles of this protein in cancer cell biology have been emerged. Indeed, it has been reported that E-cadherin can have anti-tumorigenic properties by sequestering β-catenin with activating mutations and directly interacting with extracellular growth factor receptors, such as EGFR, to suppress tumor cell proliferation[64,65].

In this respect, unlike what HaCaT showed, our results (Fig. 4) indicate that epithelial carcinoma SK-MEL-28 subjected to in vitro LIPUS exposure exhibits a significant upregulation of E-cadherin expression, while the deregulation of β-catenin is not significant suggesting that our LIPUS stimulation did not favor melanoma cell proliferation[66].

Desmosomes and cytokeratins can be oppositely modulated in non-tumorigenic HaCaTs undergoing LIPUS

It was demonstrated that desmosomes are crucial for providing epidermal adhesion and mechanical stability under stress, especially among the keratinocytes that make up the epithelial barrier. In particular, it has been reported that the modulation of the expression of proteins of the desmosome complex, such as PKP, Dsg, and desmoplakin, has effects on the enlargement or strengthening of intercellular adhesion junctions and reflects on the effectiveness of the intracellular mechanical tension sensory module (TSM)[40]. Alteration of desmosome proteins can therefore influence the expression and organization of intermediate filaments and even the organization of cortical actin filaments[39,40]. Such alterations can correspond to a transient modulation of cytokeratins to favor the elastic response dynamics: resilience, post-stress cellular repositioning, and re-epithelialization following wounding. To date, the significance of Keratin-desmosome network alterations in terms of composition and adhesion is complex and incompletely understood at a mechanistic and functional level[39,67].

Our results (Fig. 4) indicate that after one hour under LIPUS stimulus, HaCaT cells respond with a significant decrease of desmosomes and an increase in the expression level of cytokeratins compared to the

untreated control. This means that the LIPUS stimulus can affect the interaction of desmosomal components and keratins, disturbing cellular cohesion which is crucial in protecting the epidermis against various types of stress. In particular, according to our results, the "healing" response triggered by mechanical alteration capable of destabilizing the cells composing the line barrier is characterized by a transient decrease in desmosomal hyper-adhesion accompanied by an increase in the expression of keratins, i.e., K6/K16/K17 at the expense of K1/K10[67]. In this way, post-stressed keratinocytes would probably exhibit the right trade-off between mechanical resilience and increased cellular mobility. The modulation of keratins, such as K14 and K5 that are strongly involved in the mechanical absorption (together with microfilaments, and cell-edge structures), contribute to the physical resilience of keratinocytes, impacting the overall cell elasticity (i.e., Young modulus)[68]. In fact, according to previously reported nanomechanical measurements, HaCaT cells undergoing LIPUS significantly increased their stiffness[32].

It is worth stressing that in previous literature it has been documented that LIPUS can favor processes of alteration of membrane permeability and sonophoresis[69], while the role of US in accelerating processes of epithelial reformation is debated[70]. In a previous paper, some of us have highlighted that HaCaT cells subjected to similar doses of LIPUS herein involved, showed not only a change in membrane permeability but also a transient change to a less flattened shape compatible with rounding and then repositioning into the wild-type shape after tens of minutes[16]. The type of stress appears to be related to an activation of IL-6 as expected in triggering a process of keratinocyte layer restoration[71]. Despite this, the triggering of apoptotic processes has been revealed. Generally, cell rounding can be associated with several factors, among which are: apoptosis, mitosis, migration, and post-mechanical stress. The alteration in the expression of desmosomes and cytokeratins detected here on HaCaT, are compatible with the exhibited shape variations, and confirm their capability of triggering a recovery process. In this frame, our results could be a starting point for understanding the impact of LIPUS in the migration process of keratinocytes and re-epithelization.

Interestingly, LIPUS could produce changes in junction and intermediate filament proteins to trigger a series of cellular changes and wound healing resulting in an epithelial-mesenchymal transition (e.g., keratinocyte migration, loss of polarity, decrease in cell-cell adhesion, etc.). On the other hand, similar processes also occur in carcinogenesis to transform in situ melanoma into invasive and mobile melanoma. In the latter context, it is noteworthy to document herein the lack of significant alterations in desmosome and keratin expression of SK-MEL-28 undergoing LIPUS (Figs. 4 and 5).

LIPUS exposure can alter cell cycle and cell proliferation

The sensitivity to produce mitotic changes by LIPUS stressing the mitotic spindle or more globally, the network of cell junction filaments may depend on the cell cycle phase as well as the cell type. Since cells are not synchronized, we expect a multifaceted response which will turn to an average proliferation impact on the cells undergoing LIPUS. We would stress that herein we focused on evaluating the cellular response as soon as LIPUS stress ceased to document the precursory effects of long-range viability phenomena.

This working context showed that one-hour exposure to 1 MHz LIPUS produced a damage to the mitotic spindle, probably due to disassembly of the microtubules. This hypothesis is also strengthened by the increased number of treated cells undergoing pro- and metaphase (Fig. 7), showing a delay of the mitotic progression, probably due to the damage suffered by the mitotic spindle. In the case of extreme damage to the mitotic spindle (such as complete disassembly of microtubules), cells are blocked in metaphase and can exit it either through mitotic slippage or by entering apoptosis. In our case, the damage exerted to the mitotic spindle was not so drastic and thus determined a delay in the cell cycle, which in turn resulted in a decreased rate of proliferation (Fig. 6).

On the other hand, mitotic damage may result in cell death. In a previous work of our group, we have demonstrated that LIPUS exposure (65 mW/cm^2) induced the apoptosis in a small percentage of HaCaT cells[16]. Herein, we also detected the same tendency as highlighted by the increased levels of Caspase-3.

All the effects of LIPUS mentioned above concern a part of cell population that underwent the mitotic phase during the exposure. Considering that cells are not synchronized, not all of them are in mitosis during the treatment. Therefore, we believe that in non-mitotic cells the impact of LIPUS irradiation is different and affects mainly the cytoskeletal compartment, inducing the activation of signaling pathways which cooperate in a process of structural and functional recovery of cells.

Conclusions

In this work we demonstrated some short-term in vitro biological effects deriving from LIPUS mechanical stimulation and attributable to cytogenetic stress in connection with alterations of intermediate filaments and intercellular adhesion. Interestingly enough, LIPUS exposure induces different effects depending on the cell line. Both non-tumorigenic (HaCaT) and tumorigenic (SK-MEL-28) cell lines show an increase of MN + frequencies induced by one-hour exposure to 1 MHz LIPUS, also demonstrated by significant aneuploidy in HaCaT cells only. This phenomenon may be related to the oscillatory perturbation of the applied ultrasound field which seems capable of stressing the microtubule network and the arrangement of the actin filaments.

According to our results, LIPUS can in fact induce mechanical stress transmitted to the cytoskeleton and cell-junction proteins producing an alteration of cellular morphology and cell adhesion. In HaCaT cells, the alteration verified at the junction and intermediate filament level could be traced back to a recovery phenomenon (structural and proliferative) that might pass through an increased mobility and that, for analogy to what occur on tissue, could even resemble the incipit of an in vivo post-stress re-epithelialization process. In this scenario, the cellular subpopulation that responds to LIPUS-mediated mechanical stress with cytogenetic alteration could undergo cycle alteration and apoptosis, while complementary subpopulations could trigger structural and functional recovery processes. On the other hand, on LIPUS treated SK-MEL-28, we pointed out the

lack of significant deregulation in desmosome and keratin expression together with a significant increase of E-Cadherin expression. It is also worth notable that the dose-dependent decrease in SK-MEL-28 proliferation, herein reported, might deserve some biomedical attention on LIPUS as antiblastic agent.

While revealing multifaceted effects, the overall results indicate that there may be a correlation between the exhibited effects and the phase of the cycle. It should be further investigated if such an apparent comparatively lower sensitivity of SK-MEL-28 cells to LIPUS stress can turn in a lower sensitivity to sensing and transducing mechanical stress to the mitotic spindle thus affecting the micronuclei frequency. Consequently, further investigation is required to dissect the interplay between the genomic damage and the resilience response of cytoskeleton proteins during LIPUS exposure. To do this, undoubtedly it will be important to follow the impact of LIPUS in synchronized cells and at varying the exposure time. Finally, in vivo tests will be crucial to understand how the biological impact of the mechanical wave stimulation herein pointed out in vitro, and it will be disclosed in the forthcoming paper.

Data availability

The datasets generated during and/or analyzed during the current study are available from the corresponding author on reasonable request.

Received: 28 October 2024; Accepted: 29 January 2025
Published online: 10 February 2025

References

1. Miller, D. et al. Overview of therapeutic Ultrasound Applications and Safety considerations. *J. Ultrasound Med.* **31**, 623–634 (2012).
2. Izadifar, Z., Babyn, P. & Chapman, D. Mechanical and Biological effects of Ultrasound: a review of Present Knowledge. *Ultrasound. Med. Biol.* **43**, 1085–1104 (2017).
3. Magnavita, N. & Fileni, A. [Occupational risk caused by ultrasound in medicine]. *Radiol. Med.* **88**, 107–111 (1994).
4. Kumar, A. et al. Visualizing tactile feedback: an overview of current technologies with a focus on ultrasound elastography. *Front. Med. Technol.* **5**, 1238129 (2023).
5. Mitragotri, S. Healing sound: the use of ultrasound in drug delivery and other therapeutic applications. *Nat. Rev. Drug Discov.* **4**, 255–260 (2005).
6. Chang, H. et al. A bibliometric analysis for low-intensity Ultrasound Study over the Past three decades. *J. Ultrasound Med.* **42**, 2215–2232 (2023).
7. Cambier, D. et al. Therapeutic ultrasound: temperature increase at different depths by different modes in a human cadaver. *J. Rehabil Med.* **33**, 212–215 (2001).
8. Quarato, C. M. I. et al. A review on Biological effects of Ultrasounds: key messages for clinicians. *Diagnostics* **13**, 855 (2023).
9. Jiang, X. et al. A review of low-intensity pulsed Ultrasound for Therapeutic Applications. *IEEE Trans. Biomed. Eng.* **66**, 2704–2718 (2019).
10. Hornsby, T. K., Jakhmola, A., Kolios, M. C. & Tavakkoli, J. A. Quantitative study of Thermal and non-thermal mechanisms in Ultrasound-Induced Nano-drug delivery. *Ultrasound. Med. Biol.* **49**, 1288–1298 (2023).
11. Zhou, S. et al. Molecular mechanisms of low intensity pulsed Ultrasound in Human skin Fibroblasts*. *J. Biol. Chem.* **279**, 54463–54469 (2004).
12. Krasovitski, B., Frenkel, V., Shoham, S. & Kimmel, E. Intramembrane cavitation as a unifying mechanism for ultrasound-induced bioeffects. *Proc. Natl. Acad. Sci. U S A.* **108**, 3258–3263 (2011).
13. Domenici, F. et al. Structural and permeability sensitivity of cells to low intensity ultrasound: Infrared and fluorescence evidence *in vitro*. *Ultrasonics* **54**, 1020–1028 (2014).
14. Domenici, F. et al. Differential effects on membrane permeability and viability of human keratinocyte cells undergoing very low intensity megasonic fields. *Sci. Rep.* **7**, 16536 (2017).
15. Kudo, N. & Kinoshita, Y. Effects of cell culture scaffold stiffness on cell membrane damage induced by sonoporation. *J. Med. Ultrason. (2001).* **41**, 411–420 (2014).
16. Giantulli, S. et al. Effect of 1-MHz ultrasound on the proinflammatory interleukin-6 secretion in human keratinocytes. *Sci. Rep.* **11**, 19033 (2021).
17. Xu, M. et al. Review on experimental study and clinical application of low-intensity pulsed ultrasound in inflammation. *Quant. Imaging Med. Surg.* **11**, 443–462 (2021).
18. Udroiu, I. et al. Potential genotoxic effects of low-intensity ultrasound on fibroblasts, evaluated with the cytokinesis-block micronucleus assay. *Mutat. Research/Genetic Toxicol. Environ. Mutagen.* **772**, 20–24 (2014).
19. Furusawa, Y. et al. Effects of therapeutic ultrasound on the nucleus and genomic DNA. *Ultrason. Sonochem.* **21**, 2061–2068 (2014).
20. Zhou, M. et al. Effects of low-intensity ultrasound opening the blood-brain barrier on Alzheimer's disease—a mini review. *Front. Neurol.* **14**, 1274642 (2023).
21. Blackmore, D. G. et al. Low-intensity ultrasound restores long-term potentiation and memory in senescent mice through pleiotropic mechanisms including NMDAR signaling. *Mol. Psychiatry.* **26**, 6975–6991 (2021).
22. Haroon, J. et al. Use of transcranial low-intensity focused ultrasound for targeted delivery of stem cell-derived exosomes to the brain. *Sci. Rep.* **13**, 17707 (2023).
23. Liu, T. et al. Recent advances and future directions. *Brain Stimul.* **15**, 1308–1317 (2022). Sonogenetics.
24. Kamimura, H. A. S., Conti, A., Toschi, N. & Konofagou, E. E. Ultrasound neuromodulation: mechanisms and the potential of multimodal stimulation for neuronal function assessment. *Front. Phys.* **8**, 150 (2020).
25. Suresh, R., Uma Devi, P., Ovchinnikov, N. & McRae, A. Long-term effects of diagnostic ultrasound during fetal period on postnatal development and adult behavior of mouse. *Life Sci.* **71**, 339–350 (2002).
26. Bianchi, S. Ultrasound and bone: a pictorial review. *J. Ultrasound.* **23**, 227–257 (2020).
27. Lou, S., Lv, H., Li, Z., Zhang, L. & Tang, P. The effects of low-intensity pulsed ultrasound on fresh fracture: a meta-analysis. *Med. (Baltim).* **96**, e8181 (2017).
28. Ichijo, S. et al. Low-intensity pulsed ultrasound therapy promotes recovery from stroke by enhancing Angio-neurogenesis in mice in vivo. *Sci. Rep.* **11**, 4958 (2021).
29. Xu, R. S., Wu, X. M. & Xiong, Z. Q. Low-intensity ultrasound directly modulates neural activity of the cerebellar cortex. *Brain Stimul.* **16**, 918–926 (2023).
30. Schuster, A. et al. Cell specific ultrasound effects are dose and frequency dependent. *Ann. Anat.* **195**, 57–67 (2013).
31. Figarol, A. et al. Biological effects and applications of bulk and surface acoustic waves on in Vitro cultured Mammal cells: New insights. *Biomedicines* **10**, 1166 (2022).

32. Domenici, F. et al. Ultrasound well below the intensity threshold of cavitation can promote efficient uptake of small drug model molecules in fibroblast cells. *Drug Deliv.* **20**, 285–295 (2013).
33. Loria, R. et al. Very low intensity ultrasounds as a new strategy to improve selective delivery of nanoparticles-complexes in cancer cells. *J. Experimental Clin. Cancer Research: CR* **38**, 1 (2019).
34. Domenici, F. et al. Ultrasound delivery of Surface enhanced InfraRed absorption active gold-nanoprobes into fibroblast cells: a biological study via Synchrotron-based InfraRed microanalysis at single cell level. *Sci. Rep.* **9**, 11845 (2019).
35. Udroiu, I. et al. Genomic damage induced by 1-MHz ultrasound in vitro. *Environ. Mol. Mutagen.* **59**, 60–68 (2018).
36. Udroiu, I. et al. In vitro effects of 1-MHz ultrasound on the mitotic spindle. *Environ. Mol. Mutagen.* **60**, 568–575 (2019).
37. Hoffman, L. M. et al. Mechanical stress triggers nuclear remodeling and the formation of transmembrane actin nuclear lines with associated nuclear pore complexes. *Mol. Biol. Cell.* **31**, 1774–1787 (2020).
38. Shutova, M. S. & Boehncke, W. H. Mechanotransduction in skin inflammation. *Cells* **11**, 2026 (2022).
39. Hatzfeld, M., Keil, R. & Magin, T. M. Desmosomes and intermediate filaments: their consequences for tissue mechanics. *Cold Spring Harb Perspect. Biol.* **9**, a029157 (2017).
40. Aj, P. et al. Mechanical loading of desmosomes depends on the magnitude and orientation of external stress. *Nat. Commun.* **9**, 1 (2018).
41. Wang, A., Dunn, A. R. & Weis, W. I. Mechanism of the cadherin–catenin F-actin catch bond interaction. *eLife* 11, e80130.
42. Mège, R. M. & Ishiyama, N. Integration of cadherin adhesion and cytoskeleton at Adherens junctions. *Cold Spring Harb Perspect. Biol.* **9**, a028738 (2017).
43. Kelkar, M. et al. Spindle reorientation in response to mechanical stress is an emergent property of the spindle positioning mechanisms (2022).
44. Chien, W. C. & Tsai, T. F. The pressurized skin: a review on the pathological effect of mechanical pressure on the skin from the Cellular Perspective. *Int. J. Mol. Sci.* **24**, 15207 (2023).
45. le Duc, Q. et al. Vinculin potentiates E-cadherin mechanosensing and is recruited to actin-anchored sites within adherens junctions in a myosin II-dependent manner. *J. Cell. Biol.* **189**, 1107–1115 (2010).
46. Tian, X. et al. E-Cadherin/β-Catenin Complex and the Epithelial Barrier. *J Biomed Biotechnol* 567305 (2011). (2011).
47. Flitney, E. W., Kuczmarski, E. R., Adam, S. A. & Goldman, R. D. Insights into the mechanical properties of epithelial cells: the effects of shear stress on the assembly and remodeling of keratin intermediate filaments. *FASEB J.* **23**, 2110–2119 (2009).
48. di Ghelli Luserna, A., Martinelli, G. & Simonetti, G. The balance between mitotic death and mitotic slippage in acute leukemia: a new therapeutic window? *J. Hematol. Oncol.* **12**, 123 (2019).
49. Furusawa, Y. et al. DNA double-strand breaks induced by cavitational mechanical effects of ultrasound in cancer cell lines. *PLoS One*. **7**, e29012 (2012).
50. Barnett, S. Nonthermal issues: Cavitation—its nature, detection and measurement. *Ultrasound. Med. Biol.* **24**, S11–S21 (1998).
51. Hrazdira, I., Skorpíková, J. & Dolníková, M. Ultrasonically induced alterations of cultured tumour cells. *Eur. J. Ultrasound.* **8**, 43–49 (1998).
52. Skorpíková, J., Dolníková, M., Hrazdira, I. & Janisch, R. Changes in microtubules and microfilaments due to a combined effect of ultrasound and cytostatics in HeLa cells. *Folia Biol. (Praha).* **47**, 143–147 (2001).
53. Jégou, A. & Romet-Lemonne, G. Mechanically tuning actin filaments to modulate the action of actin-binding proteins. *Curr. Opin. Cell. Biol.* **68**, 72–80 (2021).
54. Russell, D., Andrews, P. D., James, J. & Lane, E. B. Mechanical stress induces profound remodelling of keratin filaments and cell junctions in epidermolysis bullosa simplex keratinocytes. *J. Cell. Sci.* **117**, 5233–5243 (2004).
55. Blase, C., Becker, D., Kappel, S. & Bereiter-Hahn, J. Microfilament dynamics during HaCaT cell volume regulation. *Eur. J. Cell. Biol.* **88**, 131–139 (2009).
56. Kim, D. & Kwon, S. Vibrational stress affects extracellular signal-regulated kinases activation and cytoskeleton structure in human keratinocytes. *PLoS One*. **15**, e0231174 (2020).
57. Rao, J. & Li, N. Microfilament actin remodeling as a potential target for cancer drug development. *Curr. Cancer Drug Targets*. **4**, 345–354 (2004).
58. Bonello, T. T., Stehn, J. R. & Gunning, P. W. New approaches to targeting the actin cytoskeleton for chemotherapy. *Future Med. Chem.* **1**, 1311–1331 (2009).
59. Bousquet, P. F. et al. Effects of cytochalasin B in culture and in vivo on murine Madison 109 lung carcinoma and on B16 melanoma. *Cancer Res.* **50**, 1431–1439 (1990).
60. Xu, X. P. et al. Structural basis of αE-catenin-F-actin catch bond behavior. *Elife* **9**, e60878 (2020).
61. Valenta, T., Hausmann, G. & Basler, K. The many faces and functions of β-catenin. *EMBO J.* **31**, 2714–2736 (2012).
62. Shah, K. & Kazi, J. U. Phosphorylation-dependent regulation of WNT/Beta-Catenin signaling. *Front. Oncol.* **12**, 858782 (2022).
63. Vlad-Fiegen, A., Langerak, A., Eberth, S. & Müller, O. The wnt pathway destabilizes adherens junctions and promotes cell migration via β-catenin and its target gene cyclin D1. *FEBS Open. Bio.* **2**, 26–31 (2012).
64. Rubtsova, S. N., Zhitnyak, I. Y. & Gloushankova, N. A. Dual role of E-cadherin in cancer cells. *Tissue Barriers*. **10**, 2005420 (2022).
65. Frixen, U. H. et al. E-cadherin-mediated cell-cell adhesion prevents invasiveness of human carcinoma cells. *J. Cell. Biol.* **113**, 173–185 (1991).
66. Sinnberg, T. et al. β-Catenin signaling increases during melanoma progression and promotes tumor cell survival and chemoresistance. *PLoS One*. **6**, e23429 (2011).
67. Loschke, F., Homberg, M. & Magin, T. M. Keratin Isotypes Control Desmosome Stability and Dynamics through PKCα. *J. Invest. Dermatol.* **136**, 202–213 (2016).
68. Biggs, L. C., Kim, C. S., Miroshnikova, Y. A. & Wickström, S. A. Mechanical forces in the skin: roles in tissue Architecture, Stability, and function. *J. Invest. Dermatology*. **140**, 284–290 (2020).
69. Park, D., Park, H., Seo, J. & Lee, S. Sonophoresis in transdermal drug deliverys. *Ultrasonics* **54**, 56–65 (2014).
70. Hill, G. E., Fenwick, S., Matthews, B. J., Chivers, R. A. & Southgate, J. The effect of low-intensity pulsed ultrasound on repair of epithelial cell monolayers in vitro. *Ultrasound Med. Biol.* **31**, 1701–1706 (2005).
71. Johnson, B. Z., Stevenson, A. W., Prêle, C. M., Fear, M. W. & Wood, F. M. The role of IL-6 in skin fibrosis and cutaneous Wound Healing. *Biomedicines* **8**, 101 (2020).

Acknowledgements

This research was realized with the financial support of INAIL, under the agreement BRiC 2019 ID 43.

Author contributions

Conceptualization and work coordination: F.D. Methodology: I.U., F.T., A.V., E.G., I.S., A.S., A.B., M.M, S.D., F.D. investigation and data analysis: I.U., F.T., A.V., E.G., D.P., L.D., C.D., A.B., F.D. Provided the equipment: G.PA., A.S., I.S., S.D., F.D. Writing - original draft: F.D., A.V., F.T. I.U. G.P.; Writing - review and editing: A.V., G.P., D.P., I.U. I.S. A.S. G.PA, M.M, S.D., F.D. Funding acquisition: F.D., A.S., I.S., M.M. All authors reviewed the manuscript.

Declarations

Competing interests
The authors declare no competing interests.

Additional information
Supplementary Information The online version contains supplementary material available at https://doi.org/10.1038/s41598-025-88569-1.

Correspondence and requests for materials should be addressed to F.D.

Reprints and permissions information is available at www.nature.com/reprints.

Publisher's note Springer Nature remains neutral with regard to jurisdictional claims in published maps and institutional affiliations.